11th World Congress on Computational Mechanics (WCCM XI)
5th European Conference on Computational Mechanics (ECCM V)
6th European Conference on Computational Fluid Dynamics (ECFD VI)
E. Oñate, J. Oliver and A. Huerta (Eds)

SIMULATION OF INTERFACIAL FLOWS USING A CARTESIAN EXPLICIT FINITE VOLUME SOLVER

A. BARDIN[*†], G. OGER[*] AND D. LE TOUZE[*]

[*] LHEEA Lab. (UMR CNRS)
LUNAM University, Ecole Centrale Nantes
1 rue de la Noë 44300 Nantes, France

[†] IRT Jules Verne
Chemin du Chaffault 44340 Bouguenais

Key Words: *Interfacial flows, Level-Set, ACLS, Pseudo-compressible*

Abstract. An explicit Cartesian finite volume method is currently under development in trhe LHEEA Lab. [1] [2]. These developments are based on a weakly compressible cell centered scheme where second-order accuracy is provided by using a MUSCL [3] scheme together with various limiters for the hyperbolic part. This paper deals with introducing the method retained for simulating interfacial flows with this model. Among the various Eulerian methods available for the simulation of interfacial flows, we compare the Level Set (LS) method [4] and the Accurate Conservative Level Set (ACLS) method [5]. These techniques are both based on the convection of a distance function following the velocity field. The LS method has many advantages in terms of interface description, access to interface properties (normal and curvature). Its main drawback relies on the possible lack of mass conservation. In order to address this problem, the ACLS method uses a hyperbolic tangent function instead of the distance function, ensuring a reduction of errors. In this paper, these two methods are compared, through four criteria: diffusion of the interface, mass conservation, accuracy and CPU performances.

1 INTRODUCTION

The Level Set method is a popular method to describe the location of the interface in multiphase computations. The interface is represented with the help of a signed distance function which is advected by the fluid velocity. This representation has the advantage of relatively simple calculations of interface normal and curvature. Another of cited advantage of the LS method is that the parallelisation is straightforward. During its advection, the level set function loses its signed distance property. Therefore a re-initialization procedure should be applied after each advection step. The deformation of the interface during this re-initialization is a well-known problem. However, the LS method has an important disadvantage; it does not conserve the mass of the two fluids. Different approaches have been developed to satisfy the mass conservation of the LS method, such as the Accurate Conservative Level Set method (ACLS) (Olsson and Kreiss, 2005), the Particle Level Set method (PLS) (Enright et al., 2002) and the Coupled Level Set Volume-Of-Fluid (CLSVOF) (Sussman and Pucket, 2000). The

added algorithmic complexity of both the PLS and the CLSVOF methods is significant. On other hand the ACLS method improves the mass conservation and keeps the simplicity of the original method.

In the present paper, a short introduction to the conservative Level Set and the ACLS methods is provided, together with their discretization is given and for the ACLS method. Then two validation test cases used to compare these methods are presented: the Zalesak's disk and the 2-D convection-stretching of a single vortex. Comparison of the LS and the ACLS methods are then provided for these cases. The compressible (hyperbolic) Cartesian Explicit Finite Volume method used in this study is then described. Finally some numerical results obtained with this scheme on a dam-break test case are presented and discussed.

2 LEVEL SET METHOD

The Level Set method relies on a signed distance function $\phi(x;t)$ for which $|\nabla\phi|=1$ [4]. The interface between the two fluids is located on the zero level of ϕ. The interface is defined by $\Gamma(t)=\{x,t: \phi(x;t)=0\}$, and divides the entire domain into two sub-domains, characterized by the sign of the level set function ϕ.

$$\boldsymbol{\phi} = \begin{cases} \boldsymbol{-d \ in \ air} \\ \boldsymbol{0 \ at \ free \ surface} \\ \boldsymbol{d \ in \ water} \end{cases} \quad \textbf{(1)}$$

Once initialized at each grid point, the continuous updating of ϕ is equivalent to the advection of the interface using equation:

$$\frac{\partial \boldsymbol{\phi}}{\partial t} + \vec{u}.\vec{\nabla}\boldsymbol{\phi} = 0 \quad \textbf{(2)}$$

Where $\vec{u}$ is the fluid velocity. As for the choice made in this study, high-order schemes can be used in order to solve this equation, namely a Weighted Essentially Non Oscillatory scheme [7] providing a fifth order in space (for regular enough functions) and a 4th order Runge Kutta scheme for the time integration.

The presence of a sheared velocity can remove or tighten contours possibly resulting in a loss of the level set properties, so that a re-initialization algorithm is necessary:

$$\frac{\partial \boldsymbol{d}}{\partial \tau} + \boldsymbol{Sign}(\boldsymbol{\phi})\frac{\vec{\nabla}\boldsymbol{d}}{\|\vec{\nabla}\boldsymbol{d}\|}.\vec{\nabla}\boldsymbol{d} = \boldsymbol{Sign}(\boldsymbol{\phi}) \quad \textbf{(3)}$$

Properties of the interface such as the local normal and curvature are easily deduced from the Level Set function, as:

$$\vec{\boldsymbol{n}} = -\frac{\vec{\nabla}\boldsymbol{\phi}}{\|\vec{\nabla}\boldsymbol{\phi}\|} \quad \textbf{(4)}$$

$$\boldsymbol{\kappa} = \vec{\nabla}.\frac{\vec{\nabla}\boldsymbol{\phi}}{\|\vec{\nabla}\boldsymbol{\phi}\|} \quad \textbf{(5)}$$

3 ACLS METHOD

The ACLS method was first proposed by Olsson and Kreiss [5] as an improved LS method to reduce mass conservation errors while keeping the simplicity of the original method. It uses a hyperbolic tangent function instead of the distance function of the original LS method:

$$\boldsymbol{\psi = 1 + tanh(\phi)} \quad \textbf{(6)}$$

This function is advected exactly as in the LS method and also need a re-initialization algorithm:

$$\boldsymbol{\frac{\partial \psi}{\partial t} + \vec{u}.\vec{\nabla}\psi = 0} \quad \textbf{(7)}$$

$$\boldsymbol{\frac{\partial d}{\partial \tau} + \nabla[d(1-d).\vec{n}] = \nabla[\varepsilon(\vec{n}.\nabla\psi).\vec{n}]} \quad \textbf{(8)}$$

This equation is advanced in pseudo-time τ, and consists in a compression term on the left hand side that aims at sharpening the profile and in a diffusion term on the right hand size ensuring of a characteristic thickness ε. Note that this equation if also written in conservative form. Resolution of advection and re-initialization equations allows the transport of the ψ=0.5 iso-surface and preserves the shape of the hyperbolic tangent profile.

4 VALIDATION AND LS/ACLS COMPARISON

4.1 Zalesak's disk

A stream function

$$\boldsymbol{\varphi(x,y,t) = \frac{-\pi}{628}(x^2 + y^2 - x - y)} \quad \textbf{(9)}$$

is imposed in a square unit domain. Initially a slotted circle of radius 0.15 is placed at the location (0.25; 0.5).

Figure **1**and

Figure **2** show the interface location after a single revolution for the LS method and the ACLS method respectively. The errors and mass losses are provided in Table 1 and Table 2.

In comparison with [6] and [8] respectively for the LS and ACLS method, we obtain here a lower error. The error decrease is stronger in the ACLS than with the LS method. For the mass loss, the same behaviour is observed: the ACLS method provides some better results with a coarser mesh than the LS method.

Figure 2 presents some default of the ACLS method which is an abnormal dissemination of the interface. Some bubbles of interface are present and are reduce with a normal from the hyperbolic tangent function.

	Level Set		ACLS	
Mesh	Error in [6]	Present error	Error in [8]	Present error
50x50	8.82e-1	6.03e-3	8.67e-3	2.44e-2
100x100	1.47e-1	2.15e-3	1.20e-3	5.91e-4
200x200	3.35e-2	9.79e-4	3.,49e-4	1.01e-8

Table 1 : Error for one revolution of Zalesak's disk

	Level Set		ACLS	
Mesh	Mass loss in [6]	Mass loss	Mass loss in [8]	Mass loss
50x50	0.46 %	0.,60 %	3.,03 %	0.47 %
100x100	0.,05 %	0.46 %	0.28 %	0.,27 %
200x200	0.02 %	0.23 %	0.04 %	0.04 %

Table 2: Mass loss for one revolution of Zalesak's disk

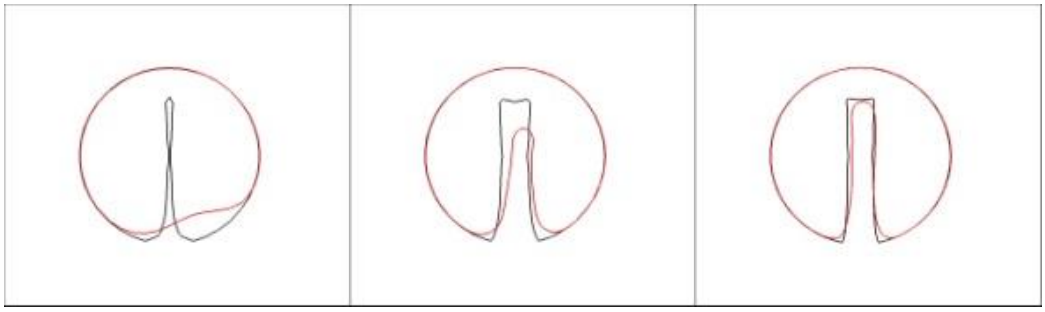

Figure 1: Level Set – Zalesak's disk after a single revolution on different grids. 50x50 (left), 100x100 (middle), 200x200 (right).

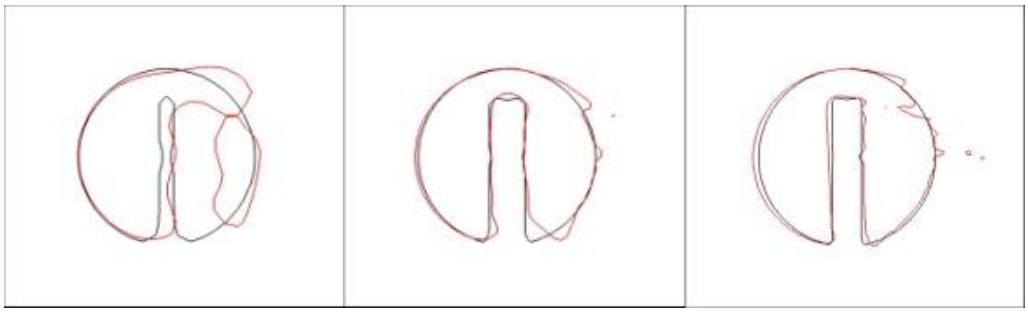

Figure 2: ACLS – Zalesak's disk after a single revolution on different grids. 50x50 (left), 100x100 (middle), 200x200 (right).

4.2 Vortex test

For this other test case, a stream function

$$\boldsymbol{\varphi(x,y,t) = \frac{1}{\pi} sin^2(\pi x) cos^2(\pi y) \cos(\frac{\pi t}{T})} \quad \textbf{(10)}$$

is imposed in a square unit domain. A circle of radius 0.15 is initially located at (0.25; 0.5). This circle is transported in the vortex and reaches its maximum deformation at t=T/2. From then on the velocity components changes their sign so that the circle finally reaches its initial position at t=T. In the literature three common values for T can be found. T=2 will not lead to very thin filaments and is therefore often used for showing the method efficiency at low resolutions. Two other values are T=6 and 8, leading to significant deformation of the circle. The contour line where ϕ=0 or ψ=0.5 at the maximum deformation is shown in

Figure 3 and

Figure 5 for three values of T for the LS method and for the ACLS method respectively. For both methods, results with a 128x128 grid are deteriorated at the tip of the form obtained. Numerical errors are characterized by losses as the line thickness becomes small. As expected, more realistic results are obtained with a 256x256 grid. Unlike for the Zalesak's disk, the velocity field is strongly sheared in this case. In these conditions, the ACLS method tends to behave better that the LS method which degrades the accuracy through a lack of control of the interface.

Figure 4 and

Figure 6 show the interface for various grid resolutions and emphasize the nice behaviour of the ACLS method compared to the LS method.

Figure 7 compares our present results for LS and ACLS methods with the results of Walker [8].

The LS method displays an important mass loss, unlike the ACLS method which tends towards the exact solution. In comparison with the ACLS from Walker, the shear flow does not introduce a small drag with our ACLS method. This fact may be due to differences in the re-initialization procedure, for which the ACLS method is rather sensitive.

Figure 8 compares the exact solution of Rider [9] with our present results of LS and ACLS methods. Here again, the ACLS method gives better results than the LS method.

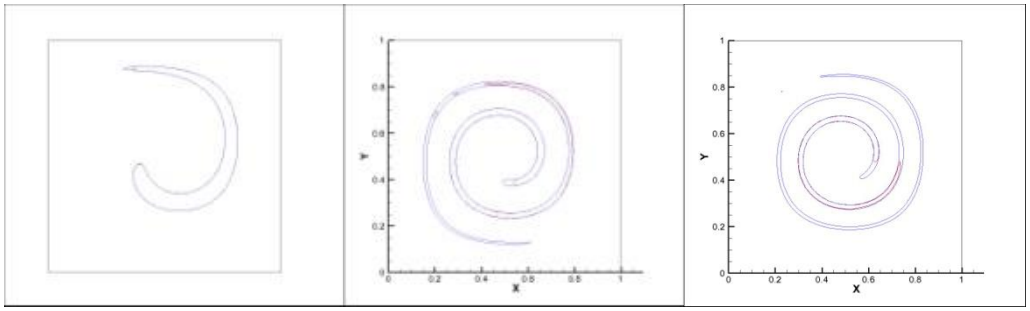

Figure 3: Level Set - Circle undergoing deformation in a vortex a t=T/2, for T=2 (left), T=6 (middle) and T=8 (right).
Red line for a 128x128 grid and Blue line for a 256x256 grid.

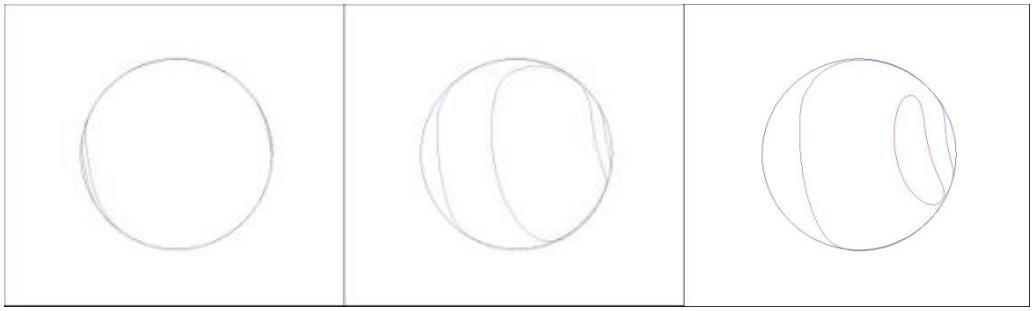

Figure 4: Level Set - Circle undergoing deformation in a vortex at t=T, for T=2 (left), T=6 (middle) and T=8 (right).
Black line: exact solution; Red line: 128x128 grid; Blue line: 256x256 grid.

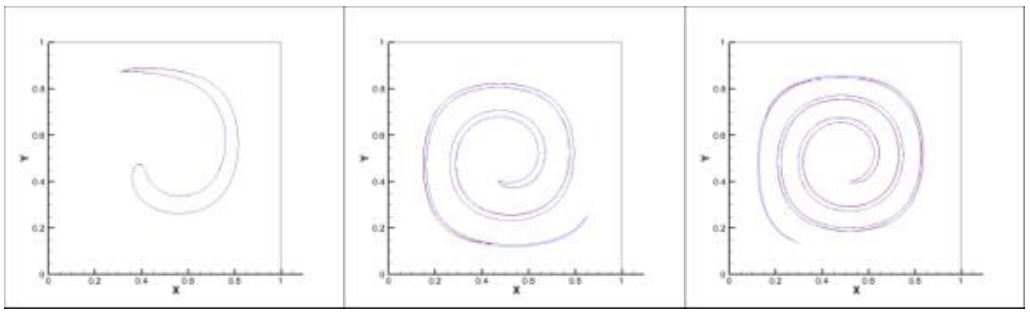

Figure 5 : ACLS - Circle undergoing deformation in a vortex at t=T, for T=2 (left), T=6 (middle) and T=8 (right).
Black line: exact solution; Red line: 128x128 grid; Blue line: 256x256 grid.

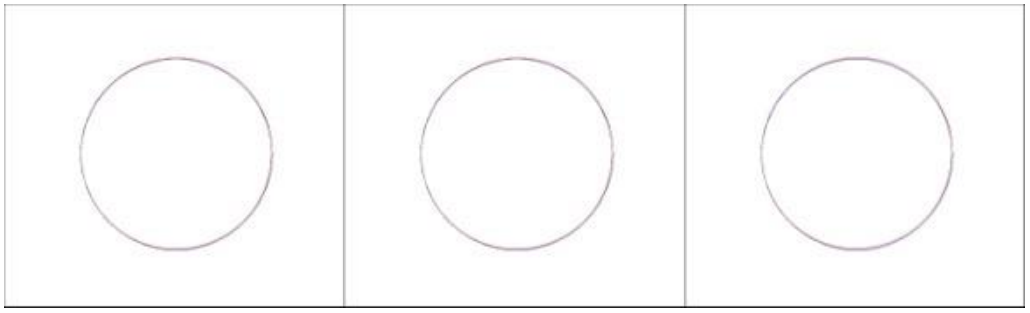

Figure 6 : ACLS - Circle undergoing deformation in a vortex at t=T, for T=2 (left), T=6 (middle) and T=8 (right).
Black line: exact solution; Red line: 128x128 grid; Blue line: 256x256 grid.

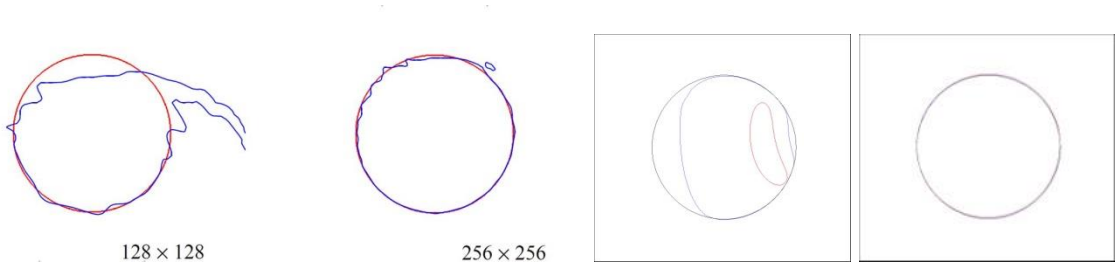

Figure 7 : Circle undergoing deformation in a vortex at t=T for T = 8s.
Results of Walker [8](left), present Level Set (middle) and present ACLS (right) for two different grid resolutions.

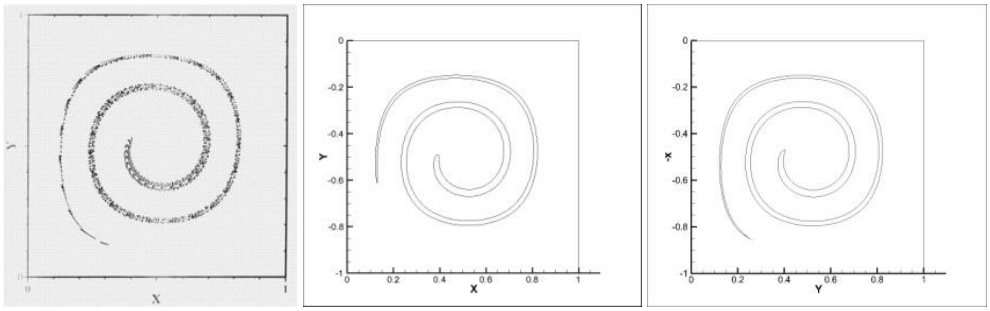

Figure 8 : Circle undergoing deformation in a vortex at t=T/2 for T = 6s.
Results of Rider [9] (left), present Level Set (middle) and present ACLS (right) for a 256x256 grid.

5 BI-PHASE FLOW MODELLING

5.1 Navier-Stokes Equations

This method solves the Navier-Stokes equations for viscous compressible flows:

$$\overrightarrow{\boldsymbol{W_t}} + \overrightarrow{\boldsymbol{\Psi(W)_{x,y,z}}} = \overrightarrow{\boldsymbol{Visc}} \tag{11}$$

To close the system and relate pressure and density, the Tait equation of state is used, thus decoupling the energy equation.

$$\boldsymbol{P - P_0 = \frac{\rho_0 c_0^2}{\gamma}\left[\left(\frac{\rho}{\rho_0}\right)^{\gamma} - 1\right]} \tag{12}$$

Where γ is the polytrophic constant, P_0 a reference pressure, ρ_0 the nominal density and c_0 the nominal speed of sound of the fluid considered.

The Navier-Stokes equations can be written in the following conservative form:

$$\begin{pmatrix}\rho\\ \rho u\\ \rho v\\ \rho w\end{pmatrix}_t + \begin{pmatrix}\rho u\\ \rho u^2 + P\\ \rho uv\\ \rho uw\end{pmatrix}_x + \begin{pmatrix}\rho v\\ \rho vu\\ \rho v^2 + P\\ \rho vw\end{pmatrix}_y + \begin{pmatrix}\rho w\\ \rho wu\\ \rho wv\\ \rho w^2 + P\end{pmatrix}_z = \overrightarrow{Visc} \tag{13}$$

The viscosity terms in Navier-Stokes equations can be represented in terms of the viscous stress tensor components:

$$\overrightarrow{\boldsymbol{Visc}} = \left(\begin{pmatrix}\boldsymbol{\tau_{xx}}\\ \boldsymbol{\tau_{xy}}\\ \boldsymbol{\tau_{xz}}\end{pmatrix}_{\boldsymbol{x}} + \begin{pmatrix}\boldsymbol{0}\\ \boldsymbol{\tau_{xy}}\\ \boldsymbol{\tau_{yy}}\\ \boldsymbol{\tau_{yz}}\end{pmatrix}_{\boldsymbol{y}} + \begin{pmatrix}\boldsymbol{\tau_{xz}}\\ \boldsymbol{\tau_{yz}}\\ \boldsymbol{\tau_{zz}}\end{pmatrix}_{\boldsymbol{z}}\right) \tag{14}$$

It can also be seen as a source term in a Laplacian operator manner, by assuming that compressibility effects in viscosity are negligible due to the weakly-compressible feature of the model.

$$\boldsymbol{F = \mu}\begin{pmatrix}\boldsymbol{0}\\ \boldsymbol{\Delta u}\\ \boldsymbol{\Delta v}\\ \boldsymbol{\Delta w}\end{pmatrix} \tag{15}$$

For solving the hyperbolic and the elliptic parts, two distinct procedures are setup and described in the next section.

5.2 Finite volume characteristic flux scheme

The formalism used in our solver is based on the Finite Volume framework, chosen to ensure the important property of conservativeness of the method. Here, the unknowns are located at the center of cells.

A new method originally developed by Ghidaglia et al. [15] in 1996 is used here. This method computes the fluxes needed at each edge by rewriting the equations with the flux Jacobian matrix and uses its hyperbolic properties. These fluxes are not expressed in terms of conservative variables as in the Godunov scheme (for instance) but directly from the physical fluxes. For more details, the reader can refer to [1][2]. The solution flux is finally expressed as follows:

$$\phi_{Solution} = \left(\frac{F(\overrightarrow{w_L}) + F(\overrightarrow{w_R})}{2} + sign(\overline{J}(\vec{w}_{\text{int}}, \vec{n})) \frac{F(\overrightarrow{w_L}) - F(\overrightarrow{w_R})}{2} \right).\vec{n} \qquad \textbf{(16)}$$

With $\overrightarrow{w_R}$ and $\overrightarrow{w_L}$ the conservative variables vector of left and right cells respectively, $\vec{w}_{\text{int}}$ the value at the interface of the two cells and $\overline{J}(\vec{w},\vec{n})$ the Jacobian matrix defined as $\overline{\overline{\boldsymbol{J}}} = \frac{\partial \boldsymbol{\Psi}(\boldsymbol{W},\vec{\boldsymbol{n}})}{\partial \boldsymbol{W}}$.

$sign(\overline{J}(\vec{w}_{\text{int}}, \vec{n}))$ is a special matrix constructed with the reduction elements of the Jacobian. This method is an alternative to Roe schemes, HLLE or AUSM+ schemes. This method is general and applicable to any hyperbolic system, easy to implement and efficient in terms of computational costs. The explicit core of the method has been validated on classical test cases. More details are provided in [2].

5.3 Weakly-compressible approach

The specificity of this method resides on the use of an explicit weakly compressible approach. Time integration is achieved using a 4$^{\text{th}}$ order Runge Kutta scheme. Stability of the scheme for solving the Euler equations is ensured by respecting the following Courant-Friedrichs-Levy (CFL) condition based on the area Γ_{int} if the interface between two adjacent cells and the speed of sound c.

$$dt \leq \min_i \left(\frac{Vol_i}{\Gamma_{\text{int}} \max_k \left| (u_i + c)_k \right|} \right) \qquad \textbf{(17)}$$

This CFL leads to possible small time steps, increasing the overall computational costs of the simulations. In order to maximize the time steps and to conserve the physical behaviour, the sound speed c_0 is chosen to be about 10 times the maximum value of velocity in the simulations. Simulations are therefore performed at Mach numbers *Ma≈0.1*. Under these assumptions, it has been shown [12] that the compressible solution can be seen as the near incompressible. Note that such approach is widely used in the SPH community for instance [13].

5.4 Interface exchanges

At the fluid-fluid interface, interfacial conditions related to velocity and pressure must be preserved (kinematic and dynamic conditions). In the present scheme the interface is treated as a contact discontinuity, so that specific flux solver is used between two adjacent cells of distinct fluid. This solver consists in a linearization of the characteristics lines from both sides of the contact discontinuity. Their intersection subsequently gives values for normal velocities and pressures at the interface [14]. The solution for normal velocity and pressure are the following:

$$\begin{cases} \boldsymbol{u^*} = \frac{\rho_L c_L u_L + \rho_R c_R u_R - (P_R - P_L)}{\rho_L c_L + \rho_R c_R} \\ \boldsymbol{p^*} = \frac{\rho_L c_L P_R + \rho_R c_R P_L - \rho_L c_L \rho_R c_R (u_R - u_L)}{\rho_L c_L + \rho_R c_R} \end{cases} \quad \textbf{(18)}$$

Both sides of the discontinuity have the same pressure (p*) and the same normal velocity (u*). The density on each side is determined by the Tait equation of state:

$$\boldsymbol{\rho = \rho_0 \left(\frac{p^*}{B} + 1\right)^{1/\gamma}} \quad \textbf{(19)}$$

With γ=1.4 for air and γ=7 for water, B is the Bulk modulus and ρ_0 the initial density of the fluid.

The solutions of this acoustic solver are used when a cell changes into another phase, i.e. when the sign of the Level Set function changes**.**

5.5 Validation of a dam-break against a wall

To validate the solver presented previously, a dam-break flow impacting a solid structure is considered. Since the Reynolds number for such an impact is generally very-high, free-slip boundary conditions are assumed. This assumption is justified by the fact that the boundary layer has a limited influence on the global flow evolution and on the pressure loads.

A sketch of this problem is shown in

Figure 9, where points *P1* and *P2* indicate the pressure probe locations. Their positions are chosen in agreement with the experiments made by Buchner [16]. This problem is studied numerically in 2D.

Figure 10 displays some snapshots of the flow evolution up to the plunging wave closure and the subsequent generation of an air bubble entrapment.

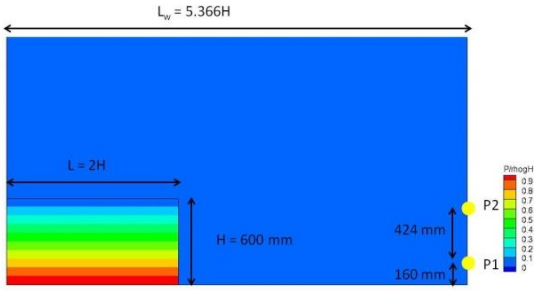

Figure 9 : Sketch of the dam-break flow against a vertical wall.
P1 and P2 are the pressure probes.

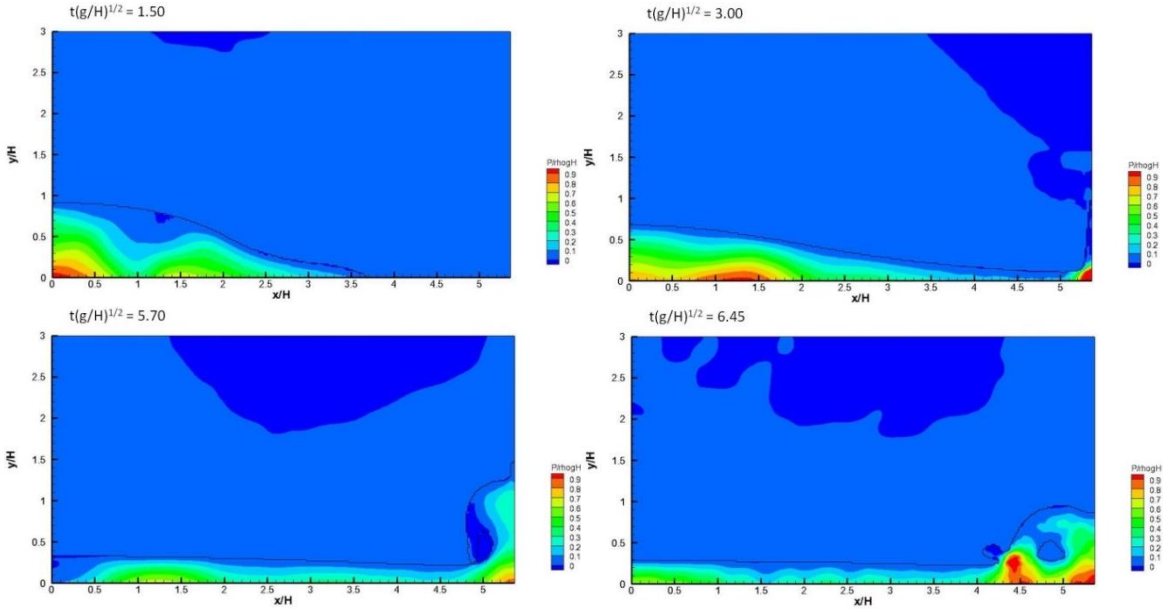

Figure 10 : Views of the evolution of the dam-break flow against a vertical wall. Results obtained with a 322x180 resolution.

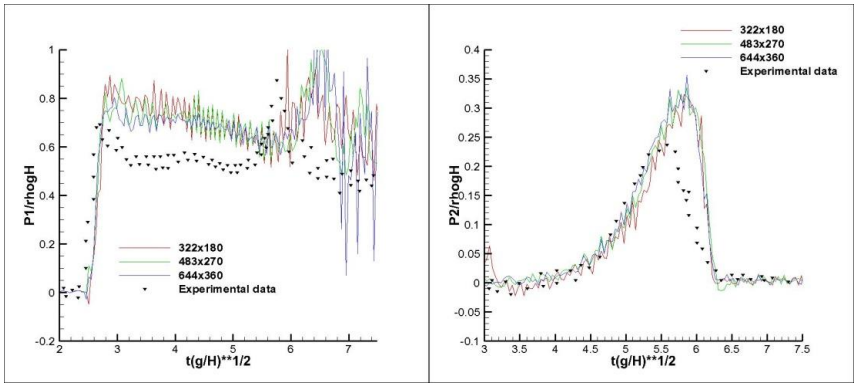

Figure 11 : Dam-break flow against a vertical wall. Comparison between the pressure loads measured experimentally and predicted by the numerical model at probes P1 (top panel) and P2 (bottom panel). Results are shown for two different space resolutions.

Comparisons on the pressure signals with the experiments by Buchner [16] are shown in

Figure **11**. The pressure signals reported are integrated on the actual probe areas. In the left panel of

Figure **11** this comparison is shown at probe P1. The agreement is not very good up to $\boldsymbol{t\sqrt{g/H} = 5.7}$. After that time, the plunging wave closes a cavity filled with air in the experiments, but computations and experiments are almost similar with a phase advance. Regarding the evolution of probe P2 plotted in the right panel of

Figure **11**, a pressure increase is observed in the experiment at about $\boldsymbol{t\sqrt{g/H} = 4.5}$ and reaches its maximum at $\boldsymbol{t\sqrt{g/H} = 5.5}$, earlier than for probe P1. The result plotted at $\boldsymbol{t\sqrt{g/H} = 5.7}$ in

Figure **12** gives an explanation for this behaviour: near the pressure probe P2, a stagnation point appears causing this pressure increase. After $\boldsymbol{t\sqrt{g/H} = 5.7}$ the numerical and experimental results are different, for the same reason as for the probe P1.

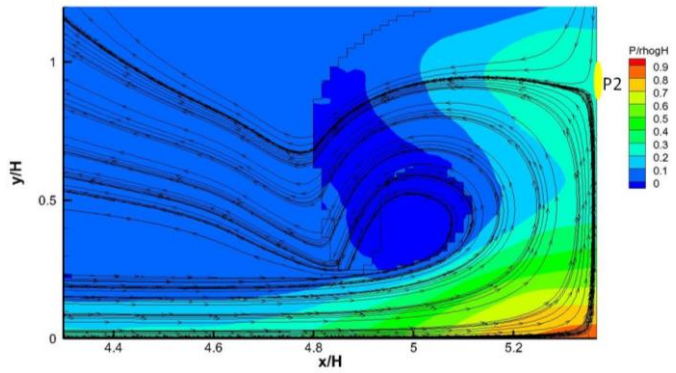

Figure 12 : Impact of the dam-break flow against a vertical wall: pressure at time $\boldsymbol{t(g/H)^{1/2} = 5.7}$ with a 322x180 discretization.

This approach combining a Level Set method and an acoustic solver gives good results in comparison with experimental data for the dam-break test case against a vertical wall.

6 CONCLUSIONS

The LS and ACLS methods have been tested and compared in this paper, in the context of a fifth order WENO and a fourth order Runge Kutta schemes respectively for the space and time discretizations. The results obtained have been compared with published solutions from Vigneaux [6], Walker [8] and Rider [9]. Good agreements have been observed for both methods. The ACLS method has better results for one test case but numerical artefacts tend to appear. These methods have been coupled in an explicit Cartesian Finite Volume solver treating the interface between fluids with fluxes defined from an acoustic solver. The results obtained with this model on a dam-break test case are very encouraging.

REFERENCES

[1] Leroy C., Bigay P., Oger G., Le Touzé D., Alessandrini B. *Preliminary developments of two-fluid Cartesian-grid Finite Volume Characteristic flux model for marine applications*. WCCM Proceedings, 2012.

[2] Bigay P., Leroy C., Oger G., Guilcher P.-M., Le Touzé D. *Development of a new cartesian explicit solver for hydrodynamics flows.* OMAE Proceedings, 2013.

[3] Van Leer B. *Towards the Ultimate Conservative DifferenceScheme. V. A Second-order Sequel to Godunov's Method.* Journal of Computational Physics, vol. 32, pp. 101-136, 1979.

[4] Osher S., Sethian J.A. *Fronts propagating with curvature dependent speed: algorithms based on Hamilton-Jacobi Formulations.* Journal of Computational Physics, vol. 79, pp. 12-49, 1988.

[5] Olsson E., Kreiss G. *A conservative level set method for two phase flow*. Journal of Computational Physics, vol. 210, pp. 210-225, 2005.

[6] Vigneaux P. *Méthodes Level Set pour des problèmes d'interface en microfluidique*. Ph.D Thesis, 2007.

[7] Ménard T. *Développement d'une méthode Level Set pour le suivi d'interface. Application à la rupture de jet liquide.* Ph. D Thesis, 2007.

[8] Walker C., Müller B. *A conservative Level Set method for sharp interface multiphase flow simulation.* ECCOMAS CFD 2010.

[9] Rider W., Kothe D. *Stretching and tearing interface tracking methods.*, 12th AIAA CFD Conference, 95-1717, 1995.

[10] Couderc F. *Développement d'un code de calcul pour al simulation d'écoulements de fluides non miscibles. Application à la désintégration assistée d'un jet liquide par un courant gazeux.* Ph. D Thesis, 2007.

[11] Fedkiw R., Aslam T., Merriman B., Osher S. *A non-oscillatory eulerian approach to interfaces in multimaterial flows (The Ghost Fluid Method*). Journal of Computational Physics, vol. 152, pp.457-492, 1999.

[12] Capdeville G. *Modélisation numérique d'écoulements compressibles, parties I et II.* Polycopié de cours de l'Ecole Centrale de Nantes, pp. 142-149, 2006.

[13] Le Touzé D., Oger G., Alessandrini B. *Smoothed Particle Hydrodynamics simulation of fast ship flows.* Proceedings of the 27th Symposium on Naval Hydrodynamics, Seoul, Korea, 2008.

[14] Murrone A. *Modèles bi-fluides à six et sept équations pour les écoulements diphasiques à faible nombre de Mach.* Ph. D Thesis, 2003.

[15] Ghidaglia J.M., Kumbaro A., Le Coq G. *Une méthode volumes finis à flux caractéristiques pour la résolution numérique des systèmes hyperboliques de lois de conservation.* C.R. Acad. Sc. Parix, Vol. 322, pp. 981-988, 1996.

[16] Buchner B. *Green Water on Ship-type Offshore Structures.* Ph. D. Thesis, 2002.